fluids

MDPI

Article

Assessing Eulerian Indicators for Predicting Mixing in a Blinking Vortex System with Varying Degrees of Continuous Transition

Hyekyung Ryu and Andrew N. Cookson *

Department of Mechanical Engineering, University of Bath, Claverton Down, Bath BA2 7AY, UK; whistle2574@gmail.com

* Correspondence: a.n.cookson@bath.ac.uk; Tel.: +44-1225-386-296

Abstract: A discontinuous change in sequential velocity fields is known to generate laminar flow mixing through the mechanism of streamline crossing. However, previous research has suggested that a small degree of continuous transition between velocity fields may not necessarily be detrimental. This study therefore used a modified blinking vortex system with varying degree of continuous transition to assess the precise effect that this continuous transition has on mixing performance. This system was studied for the parameters: blinking period, vortex spacing, and the fraction of time spent in transition. Continuous Eulerian indicators were computed to investigate their correspondence with Lagrangian-based metrics, such as Intensity of Segregation, under such conditions. The results showed that up to 30% transition time yielded improvements in mixing, most notably when vortex spacing was large, and this was consistent across different time periods. The mixing prediction by the Eulerian indicators, particularly mobility, showed good agreement with actual mixing quality, albeit not perfectly, suggesting room for refinement in these metrics. Overall, the findings imply that mixing systems, such as continuous pipe flow-based devices, which are designed assuming a discontinuous change in velocity fields, might benefit from the presence of a small degree of continuous transition between discrete states.

Keywords: blinking vortex; chaotic advection; mixing; Eulerian indicators; laminar flow; stirring; streamline crossing

Citation: Ryu, H.; Cookson, A.N. Assessing Eulerian Indicators for Predicting Mixing in a Blinking Vortex System with Varying Degrees of Continuous Transition. *Fluids* **2021**, *6*, 10. https://doi.org/10.3390/fluids6010010

Received: 4 December 2020
Accepted: 26 December 2020
Published: 30 December 2020

1. Introduction

Since Aref's [1] introduction of the blinking vortex system, discontinuous change in velocity fields, embedding streamline crossing, has been known to be an effective route to laminar flow mixing by chaotic advection. This discontinuous property has been studied in other systems such as a partitioned pipe mixer [2–5], a twisted pipe [6,7], a mixer using helical geometry [8–10], etc.

The partitioned pipe mixer devised by Khakhar et al. [2] contains two rectangular plates which are orthogonally fixed in a rotating cylinder through which fluids travel by an axial pressure gradient. The fluids are mixed not only by axially superimposed streamlines but also by the baker's transform, which squeezes/stretches fluid material elements and then cuts and stacks them to create additional layers of the different fluids [11]. This device was studied further by bifurcation analysis [3], as a generalised partitioned pipe mixer [4], and as a partitioned pipe mixer with a barrier embedded, under different rotation protocols [5].

Jones et al. [6] created a twisted pipe to induce chaotic mixing by connecting in series curved pipe segments at twist angle in the range of 0 to π. The chaotic region was found to be maximised for $\pi/2$, when streamline crossing is at a maximum. Similarly, Jen et al. [7] tested twisted microchannels in T-shaped mixers from the assumption that

chaotic advection could be achieved with a simple velocity field by periodically alternating the angle of the bottom in the channels.

An analogous effect has been implemented in curved channels and helical tubes. By changing the channel dimension or the sign of curvature, two different flow patterns are periodically switched like the blinking vortex, which generates chaotic mixing in the laminar regime without additional microstructures [8,9]. More recently, it was harnessed by Cookson et al. [10], as a way to generate enhanced mixing in a biological context, by concatenating in series small amplitude helical pipes. It had previously been found that small amplitude helical tubes induced swirling flow and in-plane mixing [12], and such effects could be enhanced by discontinuously connecting velocity fields from different helical amplitudes.

There are also other papers using the concept of blinking flow patterns. Chaotic mixing can be produced in cavity flows by alternatively moving the upper and lower walls [13], in channels by varying shape of grooves (a staggered herringbone mixer) [14], by embedding barriers [15], and by having a separatrix with secondary flows [16], and in a micromixer with two-layer serpentine crossing channels [17]. All mixing devices listed induce a periodic change in velocity fields to give the 'blinking' effect, thereby generating chaotic mixing. This effect was generalised theoretically by Sturman, Ottino, and Wiggins within the framework of Linked Twist Maps [18], which allowed for rigorous proofs of mixing bounds for simple mixing scenarios.

This discontinuous change in velocity fields is therefore clearly an important and useful mechanism for generating mixing. However, Cookson et al. [10] found that the strict discontinuity in velocity fields that was assumed for their design did not occur in practice, as there was a short distance over which a continuous transition between the vortical structures of each component pipe occurred. Comparing the mixing results to those from an idealised prediction where this discontinuity could be strictly enforced, showed very similar mixing values and Lagrangian structures, suggesting that some degree of continuous transition may not necessarily degrade the mechanism behind a discontinuous change. Only two such geometries were studied in this way, therefore leaving it unclear as to how general or robust this effect is. Furthermore, Lagrangian-based mixing analysis for optimisation in their study was computationally expensive.

Attempting to capture the principle mechanisms described in the theory of Linked Twist Maps, Sturman and Wiggins proposed Eulerian indicators (EIs) [19] as a means of predicting mixing performance from Eulerian properties alone. The EIs were refined by others [20,21] to handle continuously varying velocity fields, and may offer a route to accelerated design optimisation reducing need for Lagrangian calculations as the efficiency of the EIs has been proved in [16,19–22]. However, these metrics are not absolutely quantitative and different mixing devices are best predicted by a different subset of the Eulerian indicators.

Therefore, the aims of this study are to assess: (1) the impact, whether detrimental or beneficial, of a continuous transition regime on a mixing system designed around discontinuous operation, and (2) how well current Eulerian indicators are able to predict this mixing. As the degree of transition between velocity fields is not an independent variable in the helical pipe system, a modified blinking vortex model is chosen here as the simplest such mixing system and which gives control over this variable and others. The key findings are that continuous transition improved mixing when vortex spacing was large, but reduced mixing when vortex spacing was small. Such a trend was quite constant across different blinking periods although the effects of the vortex spacing were more noticeable for longer periods. Among the EIs investigated, mobility showed the best overall prediction of mixing quality but not for all cases, suggesting that current EIs may need further refinement.

2. Materials and Methods

2.1. Blinking Vortex with Continuous Transition

While Aref's blinking vortex model employs two point vortices which alternately turn on and off, thereby giving a discrete change in velocity fields, a continuous transition phase was introduced to that system here. Specifically, the point vortex can now move continuously with a constant velocity between the two fixed points for some or all of the total time, thus causing the velocity fields to change in a continuous, rather than discontinuous, manner. The period of the system, T, can be expressed as the sum of the time spent in the fixed state, t_{fixed}, and time spent in the transition state, t_{trans}, as follows:

$$T = t_{fixed} + t_{trans} \tag{1}$$

Figure 1a is a schematic of the blinking vortex system with the path of the moving vortex indicated. Figure 1b–d illustrate how the angle of a velocity vector at a given point (defined with respect to the positive x-axis) varies during a single period of the system. Figure 1b describes Aref's blinking vortex system, where the angle is constant for each fixed vortex, but experiences a discontinuous change at the half period. A pure transition model is described in Figure 1c where the angle continuously and linearly changes and returns to the initial point within a period. Figure 1d shows the change in angle for a system composed of both fixed and transition stages. To reflect the operating order of the fixed and moving vortex, Equation (1) can be more specifically stated as:

$$T = \frac{t_{fixed}}{2} + \frac{t_{trans}}{2} + \frac{t_{fixed}}{2} + \frac{t_{trans}}{2} \tag{2}$$

As in Aref's system, this model is two-dimensional, with the fluid both incompressible and inviscid. Particle motion is determined solely by advection via the velocity field, that is, with no diffusion. To clarify terms used in this paper, the vortex in static and transition stages will be defined as the fixed and moving vortex, respectively, and a vortex centre will represent the fixed vortex centre unless it is specified as the moving vortex centre.

2.2. Particle Tracking

Particle trajectories by the fixed vortex were computed by Aref's mapping [1]. The equation of motion for a particle in Aref's blinking vortex model is:

$$\dot{\bar{\zeta}} = \frac{\Gamma}{2\pi i} \frac{a^2 - R^2}{(\zeta - a)(a\zeta - R^2)} \tag{3}$$

where ζ, Γ, a, and R are a particle position, fixed/moving vortex strength, fixed vortex centre, and domain radius, respectively. The particle position can be expressed with its circular trajectory's centre ζ_c, radius ρ, and phase angle ϕ, as follows [1]:

$$\zeta = \zeta_c + \rho e^{i\phi} \tag{4}$$

Once the phase angle ϕ_t, after time t, is computed, the new position of the particle after t is [1]:

$$\zeta_t = \zeta_c + \rho e^{i\phi_t} \tag{5}$$

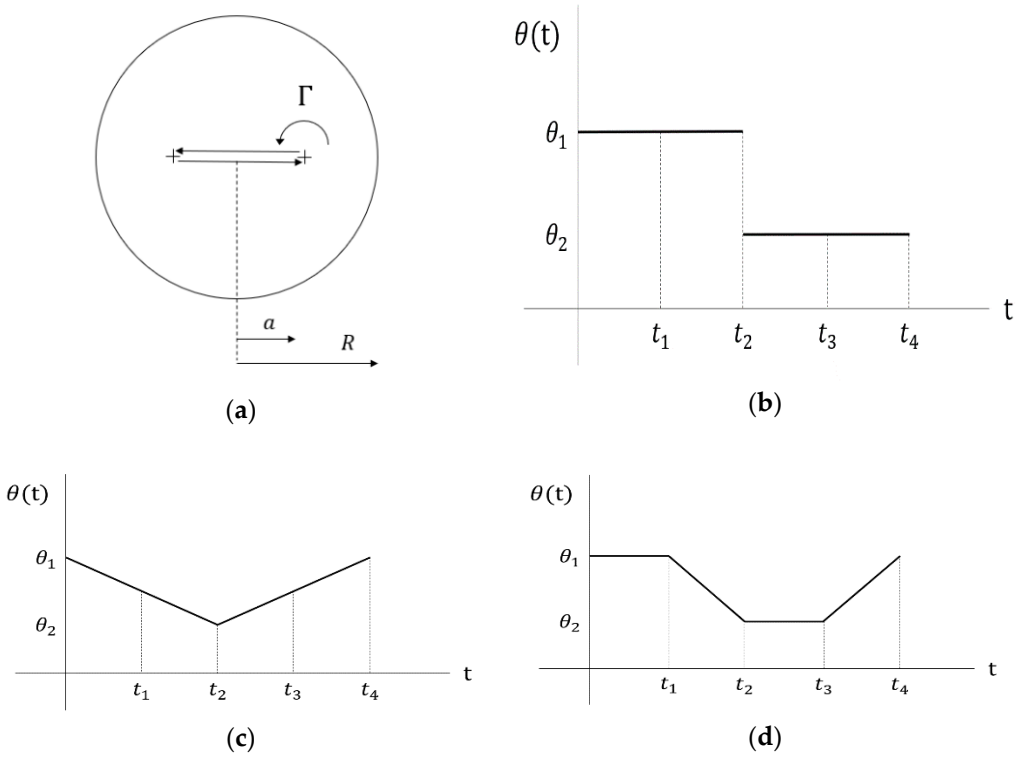

Figure 1. A schematic diagram of (**a**) Aref's blinking vortex model with moving vortex and the angle of velocity with respect to the positive x-axis for (**b**) Aref's blinking vortex model with motion of the point vortices between the fixed points of the original vortex positions; (**c**) pure transition model; and (**d**) a system with fixed and moving vortices. Γ, a, and R are vortex strength, vortex centre, and domain radius, respectively, and the arrows indicate the direction of the vortex or the trajectory of the moving vortex. A period from 0 to t_4 is not (necessarily) equally divided, but t_1 and $t_3 - t_2$ are identical and t_2 is half of t_4.

With $t_{fixed,\,1}$ and $t_{fixed,\,2}$ ($t_{fixed,\,1} = t_{fixed,\,2} = t_{fixed}/2$) being the first and second times spent in the stationary state within a period, the final particle position during the second fixed state, $\zeta_{fixed,2f}$, can be obtained using $\zeta_{fixed,1}$, which is calculated by Equation (5), without switching the vortex centre. With the initial position at $\zeta_{fixed,2i}$, the trajectory from $\zeta_{fixed,2i}$ to $\zeta_{fixed,2f}$ by the second fixed vortex is inverted against the domain centre or origin, which is identical, by symmetry considerations, to the trajectory from $-\zeta_{fixed,2i}$ to $-\zeta_{fixed,2f}$ by the first fixed vortex. The final position by the second vortex is obtained by returning $-\zeta_{fixed,2f}$ to $\zeta_{fixed,2f}$ by inversion again after $-\zeta_{fixed,2f}$ is calculated by the first vortex. The merits of this algorithm are that it does not require a generic time integration scheme for particle tracking and that its simulation time is independent of the period, which enables faster run-time independent of system parameters.

The particle trajectories during the vortex transition state are however computed by the MATLAB (Release 2019b, The MathWorks, Inc., Natick, MA, USA) functions *ode23* and *ode45*, which are three-stage and six-stage Runge-Kutta methods to solve ordinary differential equations, respectively. As the function names indicate, *ode23* and *ode45* include both second/third and fourth/fifth order methods in a single step, respectively. This dual order approach provides an error estimate that enables these adaptive time stepping schemes to achieve a specified tolerance, unless a fixed time step size is specified instead. The moving vortex centre varies over time as:

$$a_t = (-1)^{m+1} \cdot a\left(1 - \frac{4t}{t_{trans}}\right) \tag{6}$$

where

$$m = \begin{cases} odd\ numbers, & at\ the\ first\ moving\ stage \\ even\ numbers, & at\ the\ second\ moving\ stage \end{cases} \quad (7)$$

So that $a_t = a$ at $t = 0$ and $a_t = -a$ at $t = \frac{t_{trans}}{2}$ for the first half moving period, and $a_t = -a$ and $a_t = a$ for the second. Note that a_t is defined considering the code implementation, and, hence, the range of t is from 0 to $\frac{t_{trans}}{2}$, not to t_{trans}. In practice, *ode23* was used to calculate particle distributions, for reasons of computational efficiency as the difference in accuracy, compared to using *ode45*, was negligible under a small number of system iterations. However, Poincaré sections were drawn by *ode45* due to the much greater number of system iterations required to construct these plots. The time step was tested in the range 10^{-2} to 10^{-6} by 10^{-1}. When the time step is smaller than 10^{-4}, a decrease in RMS error was not noticeably reduced while the run-time significantly increased by a factor of up to 10. Both a smaller RMS error and shorter simulation time were achieved by allowing the solver to adjust the timestep automatically. The MATLAB code written for computing particle distributions, Poincaré sections, and Eulerian indicators is available for download in the Supplementary Materials.

2.3. Mixing Analysis and Prediction

2.3.1. Lagrangian Approaches

Mixing performance was evaluated qualitatively and quantitively by Poincaré sections and intensity of segregation, respectively. Poincaré sections provide a useful visualisation of structures underlying observed mixing behaviour. They represent a periodic sampling of particle trajectories across a large number of iterations. They may draw out a region of regular flow, often corresponding to a physical streamline or may have an unstructured region, generally corresponding to chaotic regions that are associated with good mixing. To create the Poincaré sections presented here, 15 particles were initially placed at $(x, y) = (\pm 0.05, 0)$, $(\pm 0.2, 0)$, $(\pm 0.35, 0)$, $(0, 0)$, $(0, 0.125)$, $(0, 0.25)$, $(0, 0.375)$, $(0, 0.5)$, $(0, 0.625)$, $(0, 0.75)$, $(0, 0.875)$, and $(0, 1)$, and the system was run for 5000 iterations.

To calculate the intensity of segregation measure of mixing, an initial distribution of red and green particles (503,424 particles in total) is perfectly segregated in the left half and right half of the domain, respectively. A grid is superimposed onto the domain, permitting a local concentration, c, to be calculated within a circle located at each grid point as [19]:

$$c = \frac{number\ of\ red\ particles}{number\ of\ red\ particles + number\ of\ green\ particles} \quad (8)$$

The circle radius was chosen as 0.04 to ensure a sufficient number of particles were included and a grid size of 0.025 was selected by running convergence tests. The average concentration over the entire domain is 0.5, with the variance of concentration across the domain given by [20]:

$$\mathcal{V}(t) = \frac{1}{N_{gridpoint}} \sum_{i=1}^{N_{gridpoint}} \left(c_i(r_i, t) - c_{avg}\right)^2 \quad (9)$$

where $N_{gridpoints}$, $c_i(r_i, t)$, and c_{avg} are the number of grid points, a local concentration at (r_i, t), and the averaged concentration over the domain, respectively. The intensity of segregation is obtained by rescaling Equation (9):

$$I = 4 \cdot \mathcal{V}(t) \quad (10)$$

A value of I equal to 0 and 1 indicates a perfect mixture of particles, and perfect segregation of particles, respectively.

2.3.2. Eulerian Approaches

The chaotic nature of particle trajectories in systems with good mixing means that time steps must in general be very small to obtain acceptable accuracy, meaning that Lagrangian analysis of mixing is usually computational expensive. Eulerian based methods of mixing performance are attractive due to their much lower computational cost. The EIs devised by Sturman and Wiggins [19] (which will be called discontinuous Eulerian indicators or d-EIs) attempted to predict mixing behaviour from several properties of the discontinuously changing velocity fields produced in a system. The velocity field in Aref's blinking vortex model is [19]:

$$\dot{x} = -\frac{\Gamma}{2\pi}\left[\frac{y}{(x-a)^2+y^2} + \frac{y}{(x-R^2/a)^2+y^2}\right] \tag{11}$$

$$\dot{y} = \frac{\Gamma}{2\pi}\left[\frac{x-a}{(x-a)^2+y^2} + \frac{x-R^2/a}{(x-R^2/a)^2+y^2}\right] \tag{12}$$

By analogy to linked twist maps, Sturman and Wiggins proposed that perpendicular streamline crossing and strong shear rate applied to adjacent fluid elements would generate good mixing. The product of those two properties showed good correspondence with the actual mixing performance, although investigating only one factor would not be enough to reflect fluid movements by the velocity fields. Note that the comparison was conducted by examining the qualitative agreement between the corresponding graphs of Lagrangian and Eulerian results, not by computing numerical errors, as the EIs only enable relative comparisons and do not provide absolute values, nor are these values within a predetermined normalised range, as is the case for intensity of segregation.

Those results, however, were dependent on a discrete change of the velocity field. Therefore, the EIs modified by McIlhany and Wiggins [20] (which will be called continuous Eulerian indicators or c-EIs) were adopted in this paper to capture the characteristics of continuously varying conditions. The c-EIs have four indicators: streamline crossing, the relative rate of velocity change, mobility, and the product of the streamline crossing and mobility. With the method being based on the time-averaged scheme,

$$\begin{aligned}\tfrac{1}{T}\textstyle\int_0^T f(t)dt = \tfrac{1}{T}\Bigg[&\textstyle\int_0^{\frac{1}{2}t_{fixed}} f_1(t)dt + \int_{\frac{1}{2}t_{fixed}}^{\frac{1}{2}(t_{fixed}+t_{trans})} f_2(t)dt \\ &+ \textstyle\int_{\frac{1}{2}(t_{fixed}+t_{trans})}^{\frac{1}{2}(t_{fixed}+t_{trans}+t_{fixed})} f_3(t)dt + \int_{\frac{1}{2}(t_{fixed}+t_{trans}+t_{fixed})}^{T} f_4(t)dt\Bigg]\end{aligned} \tag{13}$$

The integration was numerically calculated using the trapezium rule with a time step of 10^{-4}, with the singularities at the vortex centres, in Equations (11) and (12), excluded from the calculations.

The streamline crossing of the c-EIs is conceptually the same as one of the d-EIs but with a different mechanism, thereby giving the identical result for the pure blinking system. The angle of a velocity vector with respect to the positive x-axis is averaged by time as [20]:

$$\langle\theta(\boldsymbol{r};\epsilon)\rangle_t \equiv \frac{1}{T}\int_0^T \theta(\boldsymbol{r},t;\epsilon)dt \tag{14}$$

where $\boldsymbol{r}$ and ϵ include space and system parameter information, respectively. After Equation (14) is adjusted to be between $-\frac{\pi}{2}$ and $\frac{\pi}{2}$, the RMS value is computed, which is followed by the second rescaling, $\alpha(\boldsymbol{r};\epsilon)$, to make the range between 0 and $\frac{\pi}{2}$. The streamline crossing is obtained by a spatial average [20]:

$$\overline{\alpha}(\epsilon) = \langle\alpha(\boldsymbol{r};\epsilon)\rangle_r \tag{15}$$

The second indicator is computed by averaging the relative rate of velocity change over time and then on the domain, as follows [20]:

$$dw(\boldsymbol{r},t;\epsilon) = \lim_{\Delta t\to 0}\frac{||\boldsymbol{v}(\boldsymbol{r},t+\Delta t;\epsilon)-\boldsymbol{v}(\boldsymbol{r},t;\epsilon)||}{||\boldsymbol{v}(\boldsymbol{r},t+\Delta t;\epsilon)||+||\boldsymbol{v}(\boldsymbol{r},t;\epsilon)||} \tag{16}$$

$$\widetilde{w}(\boldsymbol{r};\epsilon) = \frac{1}{T}\int_0^T dw(\boldsymbol{r},t;\epsilon)dt \tag{17}$$

$$\zeta(\epsilon) = \langle \widetilde{w}(\boldsymbol{r};\epsilon)\rangle_{\boldsymbol{r}} \tag{18}$$

As for the mobility, the velocity for fast-changing flows and slow-changing flows are defined as [20,23]:

$$v_{fast}(\boldsymbol{r};\epsilon) \equiv \frac{1}{T}\left|\int_0^T \boldsymbol{v}(\boldsymbol{r},t;\epsilon)dt\right| \tag{19}$$

$$v_{slow}(\boldsymbol{r};\epsilon) \equiv \frac{1}{T}\int_0^T |\boldsymbol{v}(\boldsymbol{r},t;\epsilon)|dt \tag{20}$$

which is based on the notion that the cancellation of velocity vectors has greater importance for fast-changing flows. The integrated velocity magnitude can be expressed as [20]:

$$v_{sum}(\boldsymbol{r};\epsilon) \equiv \left(1-e^{-\widetilde{w}(\boldsymbol{r};\epsilon)}\right)v_{fast}(\boldsymbol{r};\,\epsilon) + e^{-\widetilde{w}(\boldsymbol{r};\epsilon)}v_{slow}(\boldsymbol{r};\,\epsilon) \tag{21}$$

which implies that $v_{fast}(\boldsymbol{r};\epsilon)$ is dominant with the high relative rate of velocity change while $v_{slow}(\boldsymbol{r};\epsilon)$ is the main contributor to $v_{sum}(\boldsymbol{r};\epsilon)$ with the low rate. To calculate the mobility, the threshold velocity is defined as [20,23]:

$$v_{thresh} = \left\langle \langle v_{sum}(\boldsymbol{r};\epsilon)\rangle_{\boldsymbol{r}}\right\rangle_{\epsilon} \tag{22}$$

If $v_{sum}(\boldsymbol{r};\epsilon)$ exceeds $v_{thresh}(\boldsymbol{r};\epsilon)$, $\mathbb{I}(\boldsymbol{r};\epsilon)$ is assigned a value of 1, and the mobility is computed by averaging $\mathbb{I}(\boldsymbol{r};\epsilon)$ on the domain, as follows [20]:

$$\mathbb{I}(\boldsymbol{r};\epsilon) = \begin{cases} 1 & if\ v_{sum}(\boldsymbol{r};\epsilon) \geq v_{thresh} \\ 0 & otherwise \end{cases} \tag{23}$$

$$\eta(\epsilon) \equiv \langle \mathbb{I}(\boldsymbol{r};\epsilon)\rangle_{\boldsymbol{r}} \tag{24}$$

The final indicator, $\gamma(\epsilon)$ is the product of the streamline crossing and mobility:

$$\gamma(\epsilon) = \overline{\alpha}(\epsilon)\eta(\epsilon) \tag{25}$$

2.4. Study Methods

As in Aref's paper, dimensionless parameters were defined as [1]:

$$\mu = \frac{\Gamma T}{2\pi R^2} \tag{26}$$

$$\nu = \frac{a}{R} \tag{27}$$

So that $\mu = T$ and $\nu = a$ when $\Gamma = 2\pi$ and $R = 1$, and the ratio of transition time to a period is:

$$r_{trans} = \frac{t_{trans}}{T} = \frac{t_{trans}}{\mu} \tag{28}$$

These three parameters were varied to observe their effects on mixing performance and how they interact to improve or worsen the mixing quality. The comparisons were carried out for both a fixed number of system iterations and for fixed total time ($= \mu \times iterations$). Lagrangian analysis was conducted mainly for the interpretation of the mixing behaviour

and determination of the system parameters' effects. These results were compared to the Eulerian indicator results to assess their accuracy at predicting mixing quality.

3. Results

3.1. Lagrangian Mixing Analysis

Mixing performance was evaluated for three parameters—continuous transition time (t_{trans}), vortex spacing, and blinking period—which interact with one another, thereby providing different results with a different set of the parameters. Mixing analysis was conducted with continuous transition varying either μ or ν to observe their interactions and mainly focused on phenomena occurring between the fixed vortices where the essential effect of the continuously moving vortex appears to be focused. First, the analysis was conducted comparing results from a fixed number of iterations to discover the effects of the parameters at each μ. However, as a longer period, for an equal number of iterations, gives more time for the system to mix, the effects were re-examined, keeping the total run time constant.

3.1.1. Qualitative Analysis

Before making quantitative comparisons, it is useful to compare the mixing produced in the different systems qualitatively. Poincaré sections are visually instructive for understanding and comparing the nature of the mixing behaviour of a system, particularly for identifying islands of regular flow. Figure 2 shows Poincaré sections and particle distributions for $\mu = 1$ and $\nu = 0.5$ and includes the minimum I (or the best mixing) at $r_{trans} = 0.3$ and maximum at $r_{trans} = 0.9$. From $r_{trans} = 0.0$ to 0.3, there are no significant islands of no-mixing in the Poincaré sections, only some small islands near the circular boundary. At $r_{trans} = 0.4$, however, a noticeable island appears due to overlapped analogous streamlines around the moving vortex centre, and this island grows as r_{trans} increases. The islands observed in these Poincaré sections are spatially co-located with the areas of unmixed coloured particles in the particle distribution plots, which demonstrates that the islands are functioning as a barrier to particle transport, and thus are preventing the mixing of fluid between the inside and outside of the islands. In contrast, in the chaotic regions, it is observed that particles are well mixed.

Although Poincaré sections may provide an intuitive understanding of chaotic behaviour and mixing performance, it is somewhat difficult to clearly distinguish which system produces better mixing quality when significant differences between the Poincaré sections are not readily apparent. Such differences are quantified by the intensity of segregation (in Section 3.1.2), but it remains unsolved to explain why mixing performance does not straightforwardly increase or decrease in the presence of islands. The Poincaré sections show how well particles are mixed in the system given sufficient time, but not the rate of mixing or rate of approach to an asymptotic state.

Examining the sequence of particle distributions within a single iteration reveals the physical processes that generate the fluid mixing. Figure 3 shows snapshots of the particle distributions, within one iteration, for the best mixing case (as quantified by I), that is $r_{trans} = 0.3$ with $\mu = 1$ and $\nu = 0.5$. As seen in Figure 3a, the first half period initially contributes less directly to the fluid mixing but rather acts to bring different species near to the fixed vortices. Figure 3b reveals that the second fixed vortex in the period creates circular layers of stretched material filaments around the vortex centre, which appear to be beneficial once the moving vortex is able to take particles from one side to the other (see Figure 3c,d).

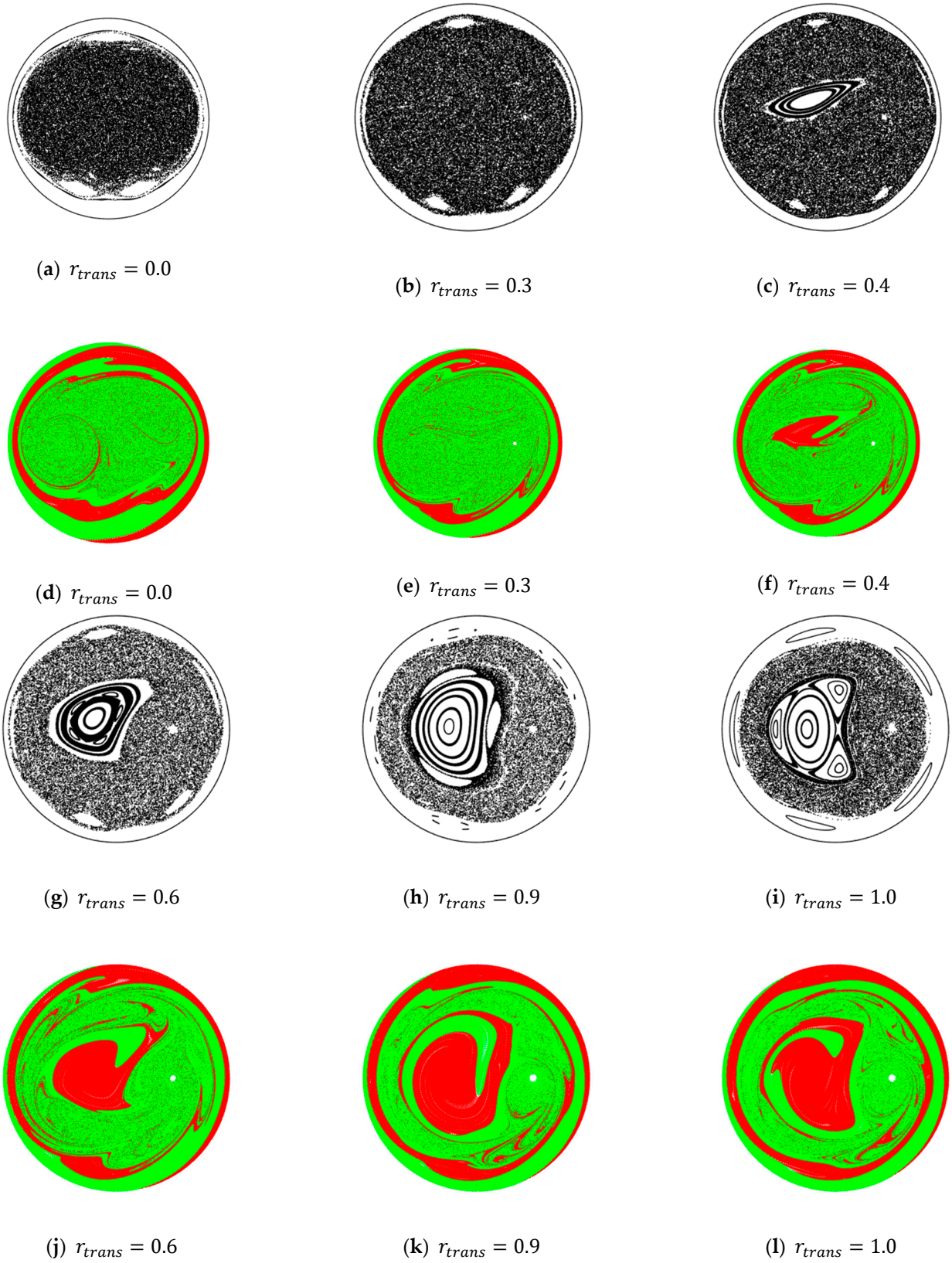

(**a**) $r_{trans} = 0.0$ (**b**) $r_{trans} = 0.3$ (**c**) $r_{trans} = 0.4$

(**d**) $r_{trans} = 0.0$ (**e**) $r_{trans} = 0.3$ (**f**) $r_{trans} = 0.4$

(**g**) $r_{trans} = 0.6$ (**h**) $r_{trans} = 0.9$ (**i**) $r_{trans} = 1.0$

(**j**) $r_{trans} = 0.6$ (**k**) $r_{trans} = 0.9$ (**l**) $r_{trans} = 1.0$

Figure 2. Poincaré sections (the first and third rows) and particle distributions (the second and forth rows) with $\mu = 1$ and $\nu = 0.5$. A total of 5000 iterations were computed to construct the Poincaré sections and the particle distribution plots experience the identical total time, equal to 10.

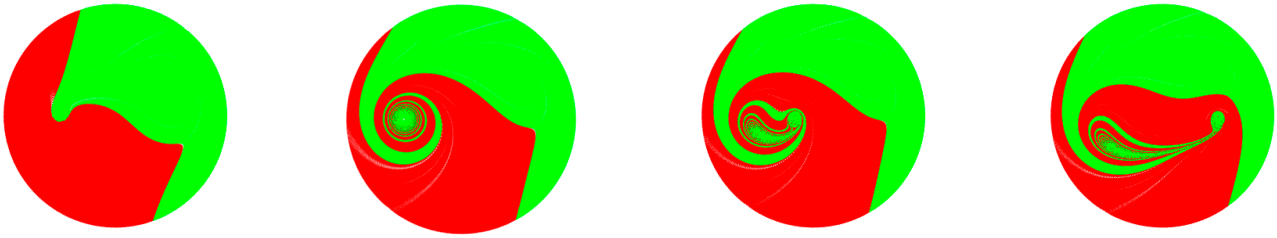

(**a**) (**b**) (**c**) (**d**)

Figure 3. Particle distribution at (**a**) t = 0.5 (half period); (**b**) 0.85 (after the second fixed vortex); (**c**) 0.9 (under moving vortex); and (**d**) 1.0 (after a single period) with μ of 1, ν of 0.5, and r_{trans} of 0.3.

The mixing performance of the system was found to depend on the ratio of t_{fixed} and t_{trans}. As the stationary vortex produces filament layers while the moving vortex transports particles between the fixed vortex centres, the system's mixing performance is reduced if the time spent in either stationary or moving regimes is too short. In Figure 4, the best mixing performance is at $r_{trans} = 0.3$ while the worst is at $r_{trans} = 0.9$. When the r_{trans} is lower than 0.3, the moving vortex cannot take particles to the other side effectively due to its near-instantaneous movements, whereas the higher r_{trans} would not allow the fixed vortex to create sufficient filament layers. Given that the fixed vortex produces no layers at $r_{trans} = 0.9$ and the moving vortex creates the layer along its trace, the pure transition is more beneficial to enhance mixing quality than r_{trans} of 0.9.

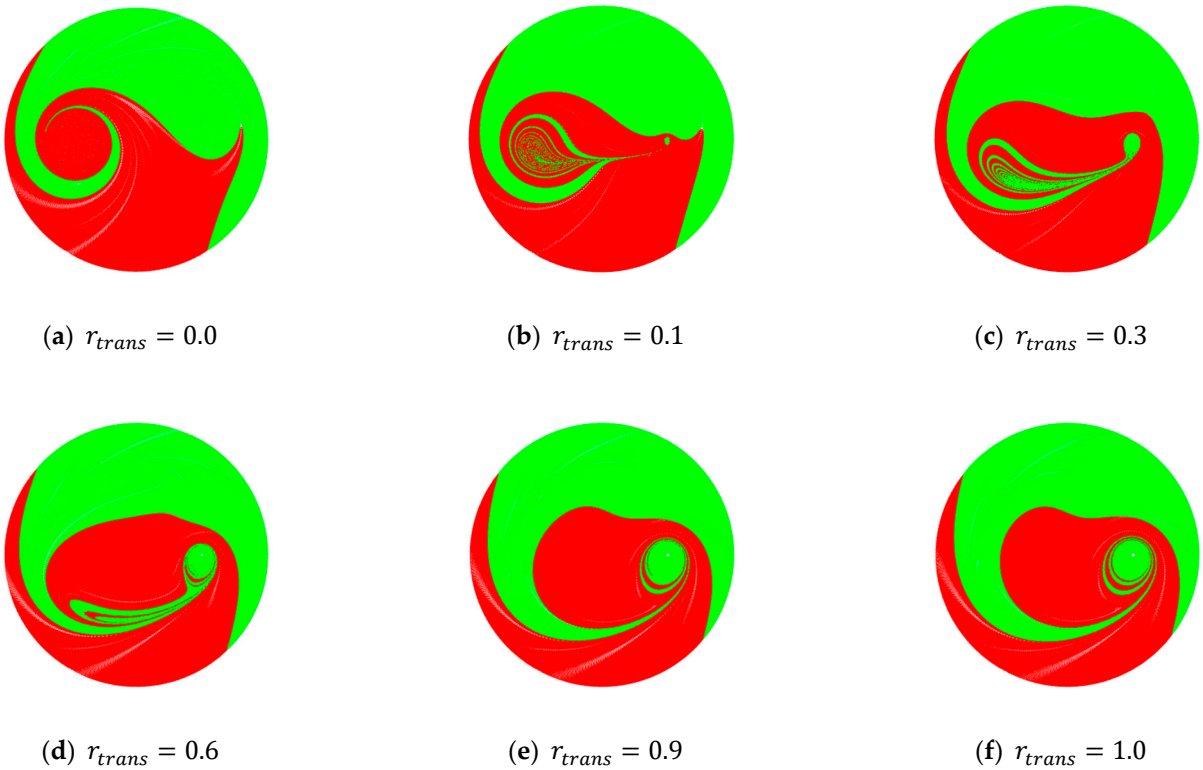

(**a**) $r_{trans} = 0.0$ (**b**) $r_{trans} = 0.1$ (**c**) $r_{trans} = 0.3$

(**d**) $r_{trans} = 0.6$ (**e**) $r_{trans} = 0.9$ (**f**) $r_{trans} = 1.0$

Figure 4. Particle distribution after one iteration with μ of 1 and ν of 0.5 with different transition time.

3.1.2. Quantitative Analysis

The coloured particle distribution plots were then analysed using the intensity of segregation metric, I, to provide a quantitative comparison of mixing performance. The effect of continuous transition and source spacing on mixing quality at each period for a fixed number of iterations of 10 is shown in Figure 5, where I is plotted against r_{trans},

varying from 0.0 to 1.0 in increments of 0.2, for different values of ν and μ. Given that a smaller value of I corresponds to better mixing performance, with the introduction of the moving vortex, the mixing quality is improved for large ν while the inverse is true for small ν. The continuous transition contributes to efficient particle transport and a decrease in discrete properties. When the vortices are adjacent, the mixing is already very effective due to the strong interactions between the point vortices, and the movement of the vortex removes the benefit of the discontinuously changing velocity fields. On the other hand, the stationary vortices positioned near the boundary (i.e., without any continuous transition) do not benefit from the discontinuous change in velocity fields due to the weak vortex interactions arising from the inverse relationship between velocity and radius. This means that the strongest part of each vortex's velocity field is in the region where only a single species (colouring) exists. This poor mixing can be enhanced by the moving vortex, which acts to physically transport particles as the vortex centre moves between the two fixed positions.

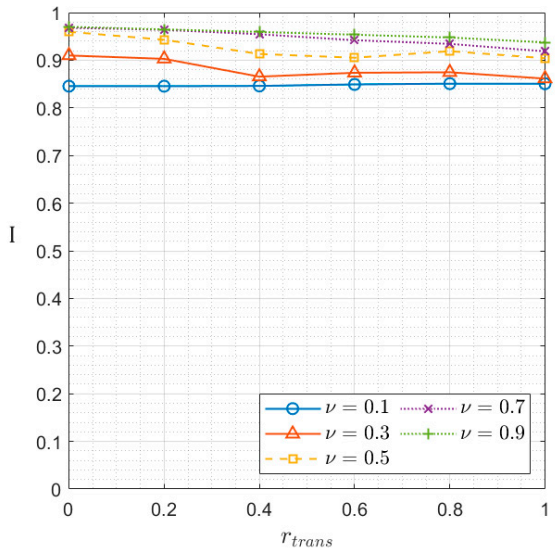

(**a**) $\mu = 0.05$

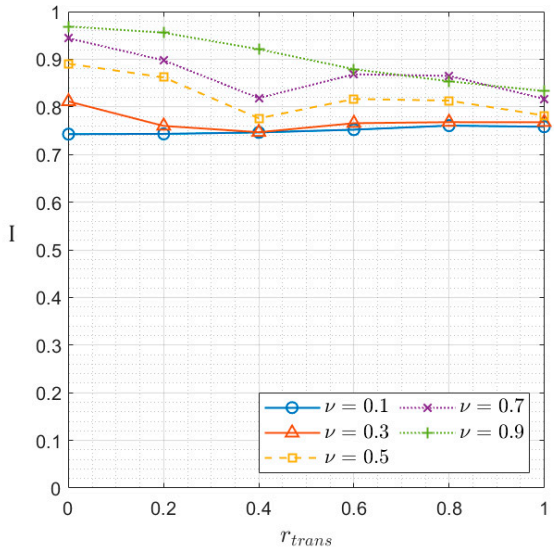

(**b**) $\mu = 0.125$

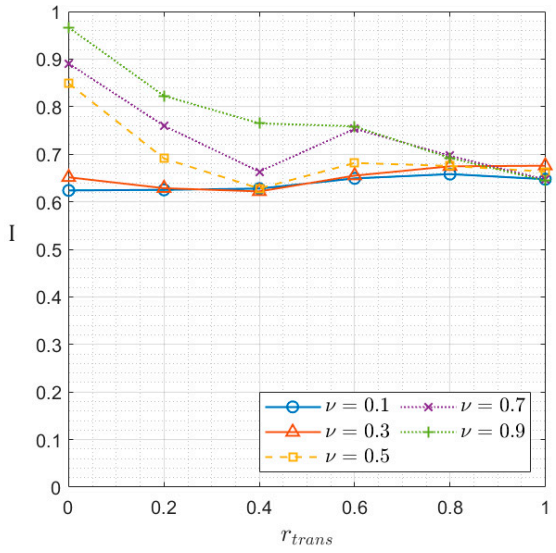

(**c**) $\mu = 0.25$

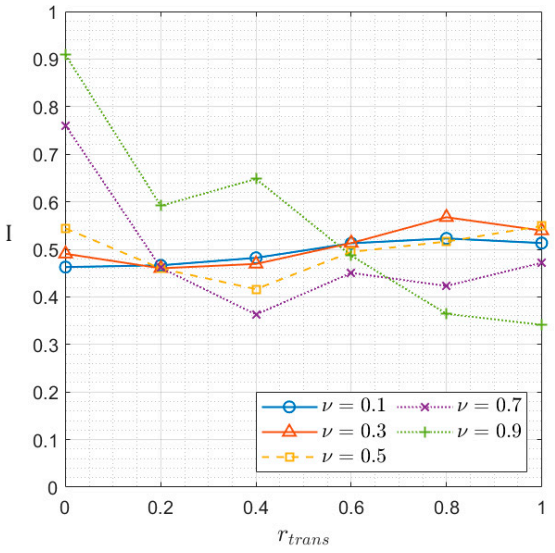

(**d**) $\mu = 0.5$

Figure 5. *Cont.*

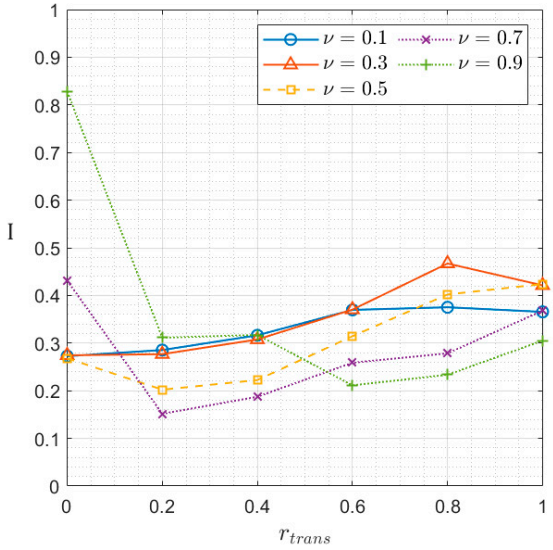

(**e**) $\mu = 1.0$

Figure 5. The effect of the transition time (r_{trans}) and fixed vortex centre (ν) on mixing performance (I) with fixed iterations of 10, which indicates that (**a**) total time is 0.5; (**b**) 1.25; (**c**) 2.5; (**d**) 5; and (**e**) 10 with different periods (μ).

Another feature of Figure 5 is that the longer period produces better mixing quality when comparing across a fixed number of iterations; for example, the performance with ν of 0.1 (blue lines in Figure 5) is improved as μ increases, which is also true for other cases. However, it does not guarantee that long periods are beneficial for mixing, in that the total time that each system experiences is different for the same number of iterations. For instance, the total time is only 0.5 for the shortest period while it is 10 for the longest of those studied here. Therefore, the better mixing performance may simply be caused by the longer total time that the system operates for and so results will also be compared for fixed total time.

The results with the same set of parameters but now with the fixed total time (equal to 10), are found in Figure 6 where the trend observed for fixed total iterations is no longer always the case. It is still true for low r_{trans}, but the improvements can be achieved with short μ as r_{trans} increases with exceptions for the large spacing. Since the mixing behaviour with zero transition is governed by discrete properties, that is streamline crossing, it is more beneficial to specify a long time period, so that a particle can escape from its previous streamline and then travel in a different direction on a new streamline as in Aref's system. In contrast, the system with pure transition is wholly driven by the moving vortex; thus, the more frequently the moving vortex stirs the fluid or the region between the fixed vortex centres experiences the stronger regions of the velocity fields, the better mixing quality can be obtained. However, the trend does not hold for the combination of large spacing and small period. In Figure 6e, an I of 0.3052 with $\mu = 1.0$ improves to 0.1099 with $\mu = 0.25$ in Figure 6c, but worsens to 0.2335 when $\mu = 0.05$ in Figure 6a. As shown in Figure 7a–f, increasing the system period produces larger islands of regular flow, thereby producing an unmixed area. The same appears the case for the large source spacing in Figure 7g–i where the island at the domain origin becomes large as μ increases. In Figure 7g, however, the seemingly chaotic region actually consists of many small-scale islands which trap particles inside separating them from the rest of the domain. Although this may be difficult to discern in a Poincaré section created with a full set of sample particles, it was found that the large chaotic regions were indeed divided into smaller chaotic regions when the Poincaré sections were created from a single particle in turn. Figure 7j shows the resultant patterns of layers of unmixed particles separated by such areas.

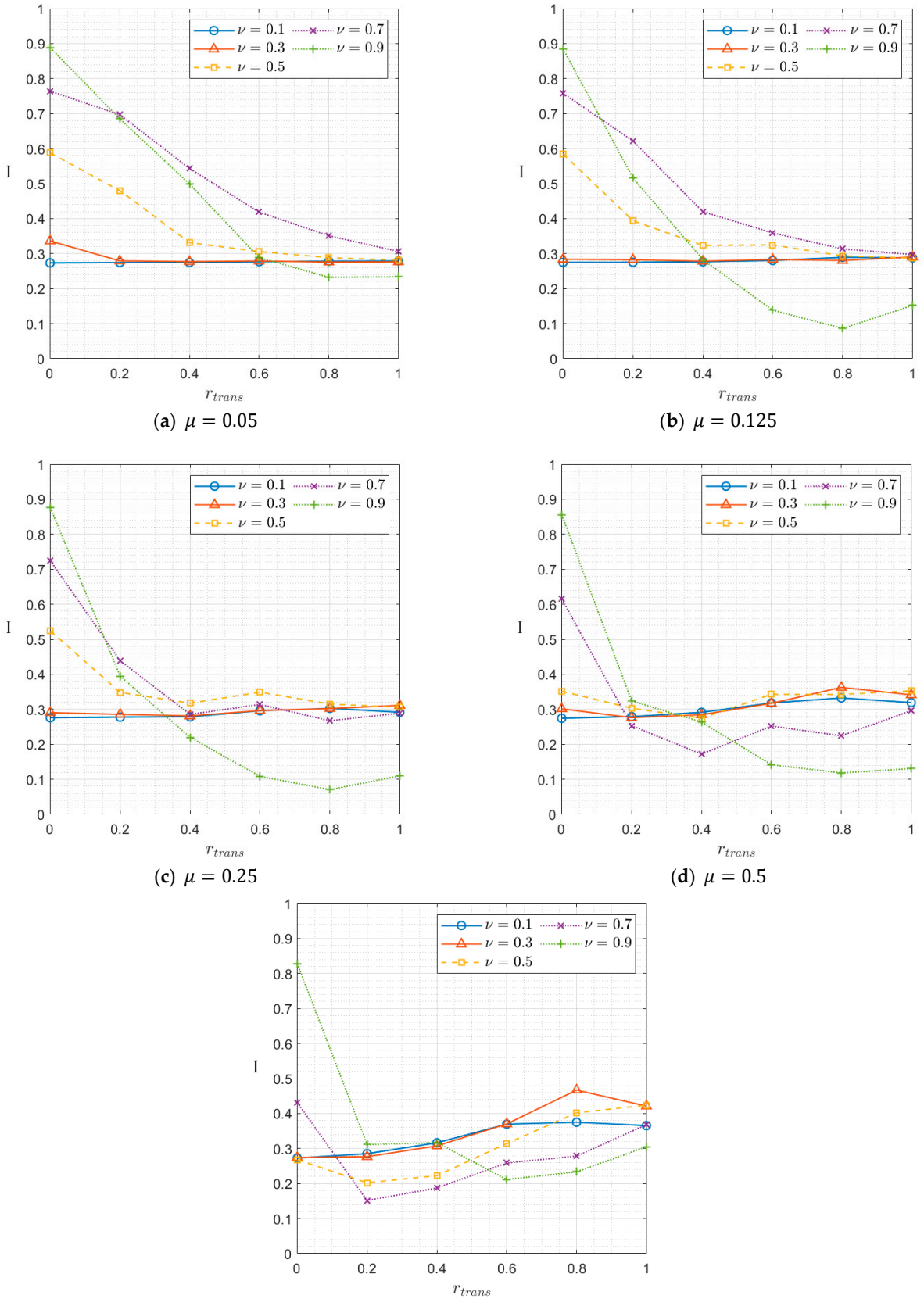

(**a**) $\mu = 0.05$ (**b**) $\mu = 0.125$

(**c**) $\mu = 0.25$ (**d**) $\mu = 0.5$

(**e**) $\mu = 1.0$

Figure 6. The effect of the transition time (r_{trans}) and fixed vortex centre (v) on mixing performance (I) with fixed total time of 10, which indicates that (**a**) iterations are 200; (**b**) 80; (**c**) 40; (**d**) 20; and (**e**) 10 with different periods (μ). Note that Figure 6e is identical to Figure 5e.

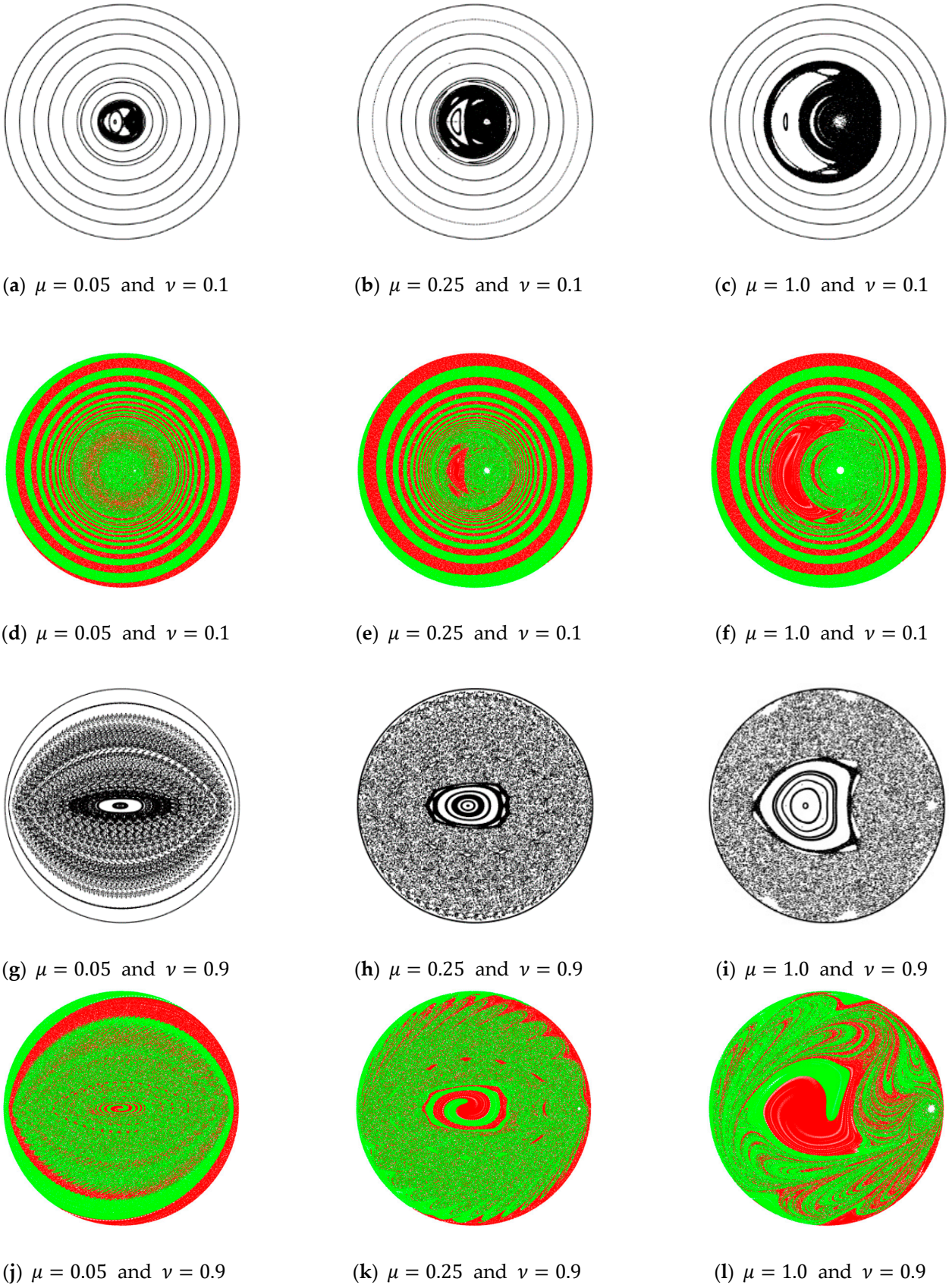

(**a**) $\mu = 0.05$ and $\nu = 0.1$ (**b**) $\mu = 0.25$ and $\nu = 0.1$ (**c**) $\mu = 1.0$ and $\nu = 0.1$

(**d**) $\mu = 0.05$ and $\nu = 0.1$ (**e**) $\mu = 0.25$ and $\nu = 0.1$ (**f**) $\mu = 1.0$ and $\nu = 0.1$

(**g**) $\mu = 0.05$ and $\nu = 0.9$ (**h**) $\mu = 0.25$ and $\nu = 0.9$ (**i**) $\mu = 1.0$ and $\nu = 0.9$

(**j**) $\mu = 0.05$ and $\nu = 0.9$ (**k**) $\mu = 0.25$ and $\nu = 0.9$ (**l**) $\mu = 1.0$ and $\nu = 0.9$

Figure 7. Poincaré sections (the first and third rows) and particle distributions (the second and forth rows) for $r_{trans} = 1$. A total of 5000 iterations were computed to construct the Poincaré sections and the particle distribution plots experience the identical total time, equal to 10.

In both Figures 5 and 6, the effect of vortex spacing appears to be qualitatively the same across the plots. The results for the pure blinking model agree with those of [1,19], that is, the conclusions that longer periods and small source spacing enhance mixing performance. As the total time of system operation is longer in the plots of Figure 6 (except for μ of 1.0 when it is equal), the results in Figure 6 reveal better mixing performance than the corresponding plots in Figure 5. Specifically, for large vortex spacing running the system for more iterations only improves mixing by less than 10%, whereas the mixing performance can be improved by up to 68% for small vortex spacing, for the pure blinking model. Vortices with a large spacing do not interact effectively (unless some continuous transition has been introduced), such that additional iterations provide little benefit. Furthermore, it is more noticeable in Figure 6 that the positive correlations between I and r_{trans} for small v do not reveal noticeable differences, compared to the broad source spacing. The continuous transition has relatively little effect on the mixing performance for small spacing while a sharp drop in I is found with even a small fraction of transition time for large spacing, as the inefficiency of the largely spaced vortex system can be significantly improved by the moving vortex. If the transition time is long enough to give the effects described in Figure 3c,d, increasing r_{trans} becomes less important afterwards. However, as for short μ, the transition time is also short in absolute terms, so the effect of r_{trans} is less significant than for long μ.

3.2. Eulerian Mixing Analysis

3.2.1. Discontinuous Eulerian Indicators

The tests with the d-EIs varying the vortex centre at different r_{trans} showed good prediction by the product of streamline crossing and shear rate, but only when the system was operated by a pure blinking vortex. With continuous transition introduced, the agreements with the actual mixing performance were mainly eliminated. The d-EIs, which capture discrete properties, were no longer suitable once r_{trans} was greater than 0.2; therefore, the c-EIs were chosen for the more thorough investigation into how to predict mixing performance for these cases. Figure 8 compares the mixing prediction of the d-EIs and c-EIs. Even in the case of the pure blinking model without continuous transition, the c-EIs provide a better prediction, albeit only for mobility.

3.2.2. Continuous Eulerian Indicators

Table 1 summaries a qualitative assessment of the strength of the correlation between various Eulerian indicators and intensity of segregation, for a range of values of vortex centre and period. The correlation was classified as Poor (P), Medium (M), and Good (G), with each table cell representing a graph of the intensity of segregation, (I) (left y-axis) and one of the Eulerian indicators ($\overline{\alpha}$, ζ, η, or γ) (right y-axis) versus the ratio of continuous transition (r_{trans}). Minor or localised discrepancies were ignored when the mixing quality was assessed as Good. For instance, the evaluation of the first plot in Figure 9a is found in Table 1 with μ of 0.05 and ν of 0.1, which is the upper left box for streamline crossing, denoted as G. Due to the c-EIs not being an absolutely quantiative measure, each evaluation was conducted with qualitative criteria instead of computing numerical errors. If the overall trend between the Lagrangian and Eulerian results was agreed, it was assessed as Medium, and if not, it was classed as Poor. Only when both the overall trend and the shape of the graph were in general agreement was the prediction classified as Good. Some examples for the classifications can be found by comparing Table 1 and Figures 9 and 10. Note that the y-axis of the c-EIs, whose correlation with mixing performance is positive, has been reversed to make clearer that the agreement with intensity of segregation indicates that the particular c-EI is a good predictor of mixing.

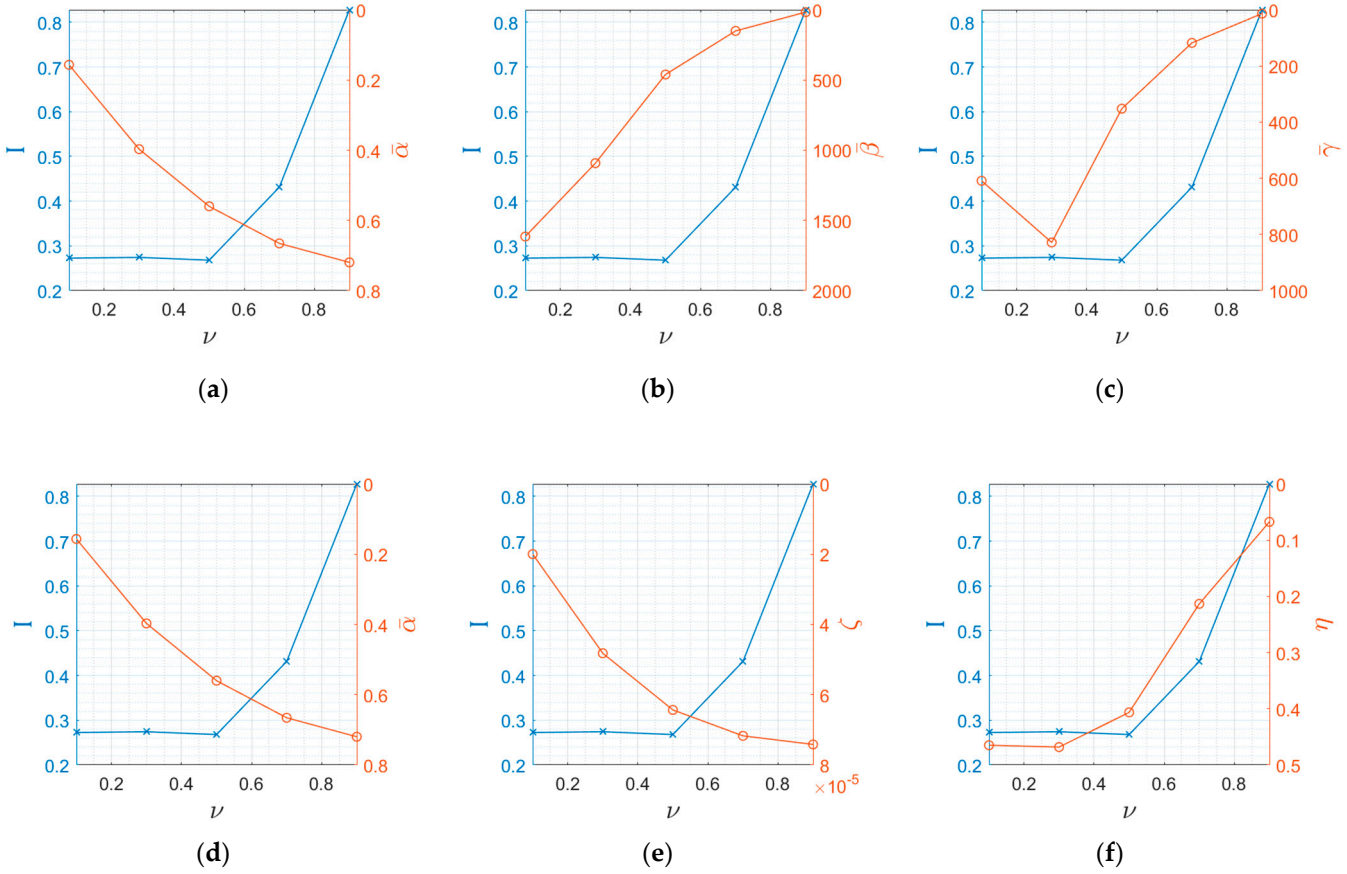

Figure 8. Comparison between d-EIs (the first row) and c-EIs (the second). The indicators are (**a**) streamline crossing; (**b**) shear rate; (**c**) the product of the streamline crossing and shear rate; (**d**) streamline crossing; (**e**) the relative rate of velocity change; and (**f**) mobility.

In Table 1, patterns dividing the classifications can be found for streamline crossing and relative rate of velocity change, although the patterns are less obvious for both mobility, and the product of streamline crossing and mobility. Configurations with the fixed iterations, denoted in the round brackets, are found not to significantly alter the trend with the fixed total time; that is, such variations do not appear globally and there were no jumps between the highest and worst assessment. In terms of the vortex spacing, it can be roughly said that the mixing performance would become worse for the small spacing while it would be improved for the large spacing as the ratio of continuous transition increases; therefore, in this case, the values of I and the c-EIs should increase and decrease, respectively, when the vortices are close, and vice versa.

For the first c-EI, streamline crossing, increasing continuous transition eliminates the discrete change of velocity fields, so perpendicular streamline crossing rarely occurs. To be more specific, the effect of the continuous transition can be interpreted as either positive or negative with respect to the angle of velocity vectors. Note that the streamline crossing metric only views the perpendicular angle as beneficial without considering the direction of velocity vectors. The angle between the velocities by two fixed vortices is almost 90° just above/below each vortex centre; for example, above the left vortex centre, the velocity by the left vortex is horizontal while one by the right vortex is almost vertical. This should be beneficial for the pure blinking model, but the angle would be divided into smaller angles with the continuous transition, meaning continuous transition has a negative effect on mixing around the vortex centres. On the other hand, the direction of the velocities between the vortex centres is almost opposite just over/below the x-axis. By dividing this angle, it can be reduced to close to 90° when only one single point of the transition is considered. Although the continuous transition would not cause the angle to be divided

into approximately two right angles, it still gives a positive influence, meaning continuous transition has a positive effect on mixing between the vortex centres. Between the vortex centres, however, the velocity vectors by the left/right vortices and transition are aligned vertically on the x-axis and around the domain centre, meaning a roughly neutral effect around the domain centre. Thus, the value of streamline crossing is always small regardless of the continuous transition. When the fixed vortices are adjacent, the effect between the centres is negligible and therefore the negative effect of continuous transition dominates the calculation, thus decreasing $\overline{\alpha}$ for small vortex spacing, while both positive and negative effects combined effects are detected for a larger vortex spacing. As the region between the fixed vortices is larger, the positive effects spread first until the expansion is prohibited by the domain centre, and the value starts to decrease by the negative effects around the vortex centres (see Figure 11a–c).

Table 1. Comparisons between Lagrangian and Eulerian results for fixed total time. The agreements are assessed as Poor (P; yellow, overall trend disagreed), Medium (M; green, overall trend agreed), and Good (G; blue, overall trend and the shape of graph agreed). The indicators in parentheses represent the corresponding results for the case of fixed iterations, where this is different to the trend for fixed total time.

		μ				
		0.05	**0.125**	**0.25**	**0.5**	**1.0**
Streamline crossing						
	0.1	G(M)	M(G)	M	G(M)	G
	0.3	P	P	M(P)	M	G
ν	0.5	P	P	P	P	M
	0.7	P	P	P	P	P
	0.9	P	P	P	P	P
Relative rate of velocity change						
	0.1	P	P	P	P	P
	0.3	M(P)	P	P	P	P
ν	0.5	M	M	M	P	P
	0.7	G	G(M)	M	M	P
	0.9	G	M(G)	M(G)	M(G)	M
Mobility						
	0.1	G(M)	M(G)	M	M	M
	0.3	P	P	M(P)	M	G
ν	0.5	G	G	G	P	P
	0.7	G	G(M)	M	M	P
	0.9	M(G)	M(G)	M	M(G)	M
Product of streamline crossing and mobility						
	0.1	G(M)	M(G)	M	**G(M)↑**	**G↑**
	0.3	P	P	M(P)	M	G
ν	0.5	**P↓**	**P↓**	**P↓**	**M↑**	**M↑**
	0.7	G	G(M)	M	M	P
	0.9	M(G)	M(G)	M	M(G)	M

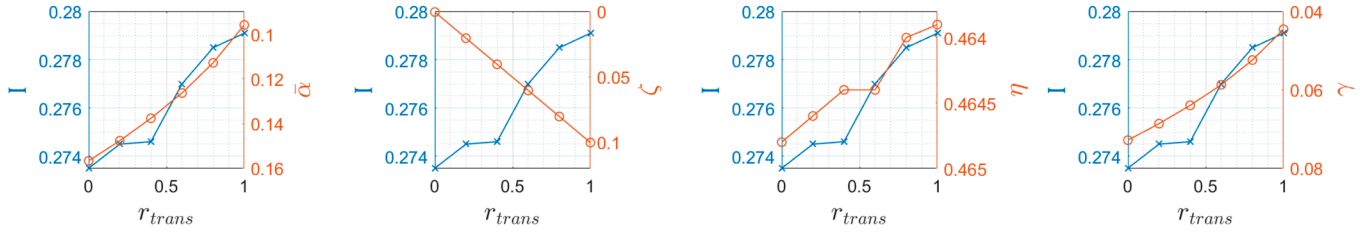

(**a**) $\nu = 0.1$

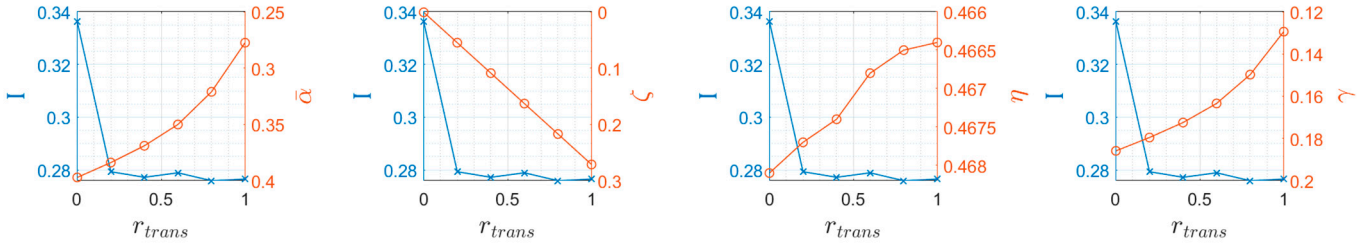

(**b**) $\nu = 0.3$

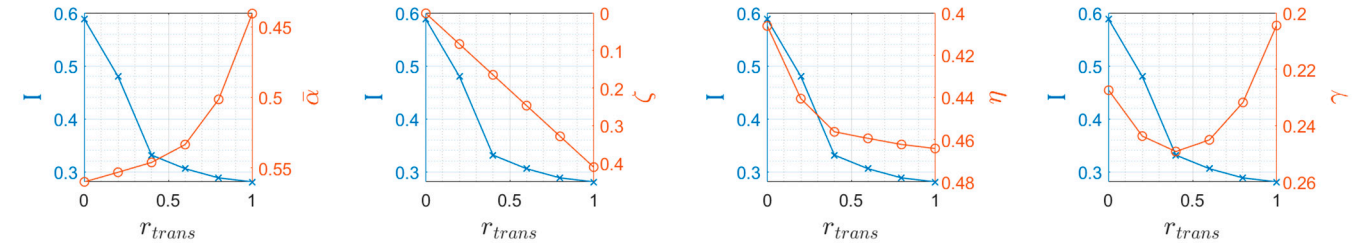

(**c**) $\nu = 0.5$

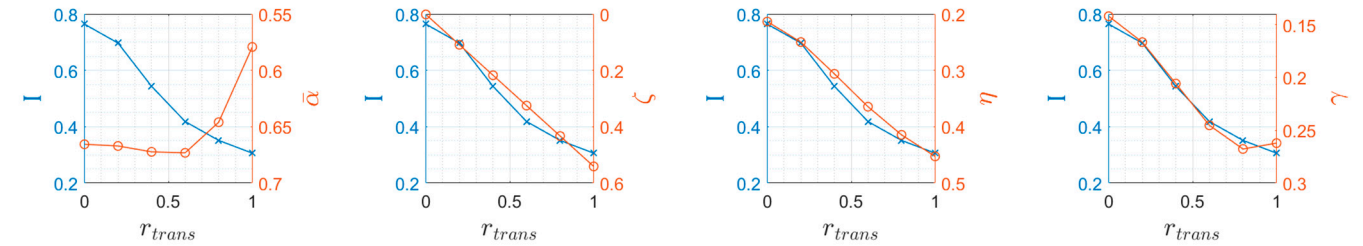

(**d**) $\nu = 0.7$

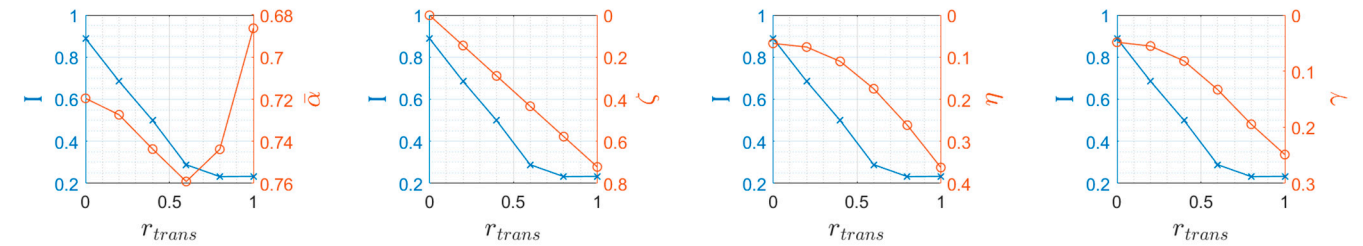

(**e**) $\nu = 0.9$

Figure 9. Comparison between I (blue lines) and c-EIs (orange lines) with μ of 0.05. From the left, the indicators are streamline crossing, the relative rate of velocity change, mobility, and the product of streamline crossing and mobility. The intensity of segregation was calculated with the identical total time, equal to 10.

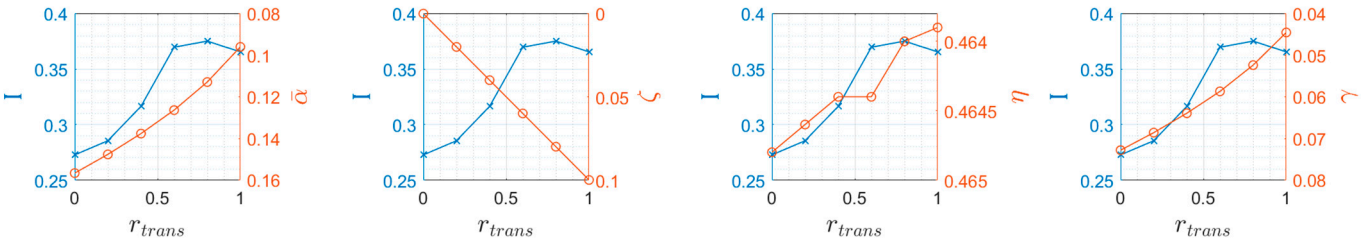

(**a**) $\nu = 0.1$

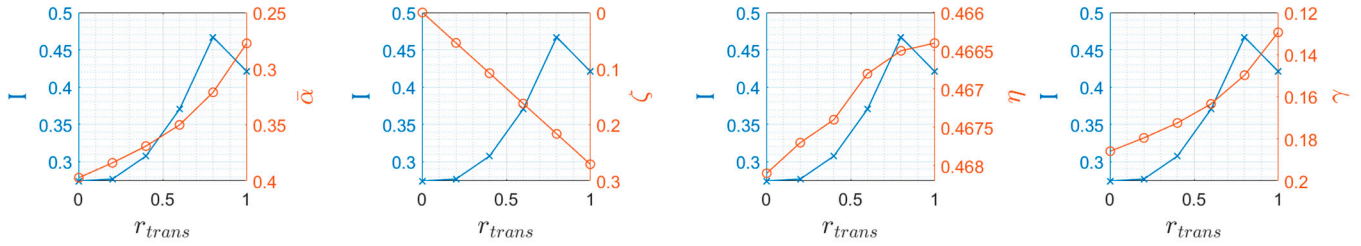

(**b**) $\nu = 0.3$

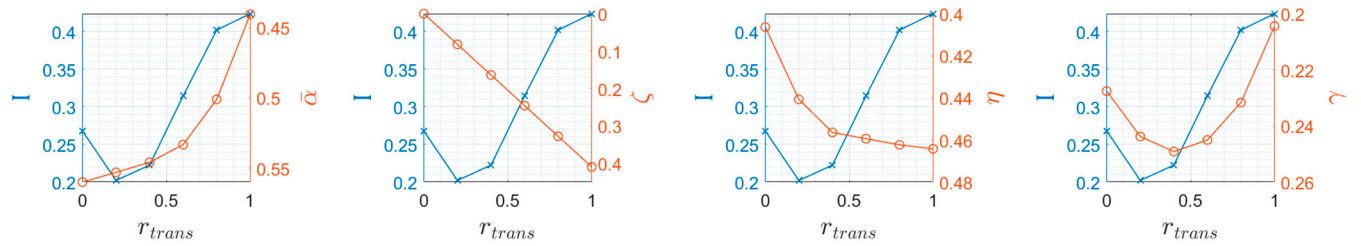

(**c**) $\nu = 0.5$

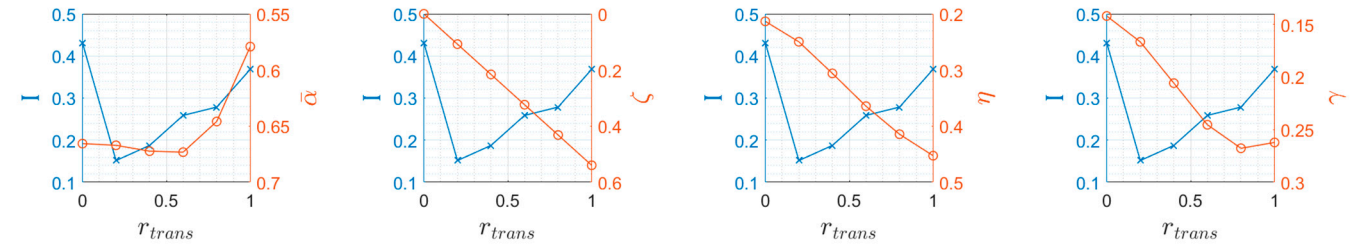

(**d**) $\nu = 0.7$

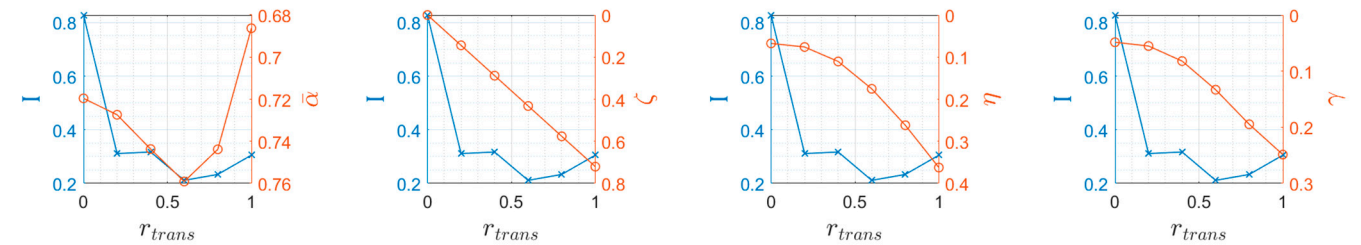

(**e**) $\nu = 0.9$

Figure 10. Comparison between I (blue lines) and c-EIs (orange lines) for $\mu = 1.0$. From the left, the indicators are streamline crossing, the relative rate of velocity change, mobility, and the product of streamline crossing and mobility. The intensity of segregation was calculated with the identical total time, equal to 10.

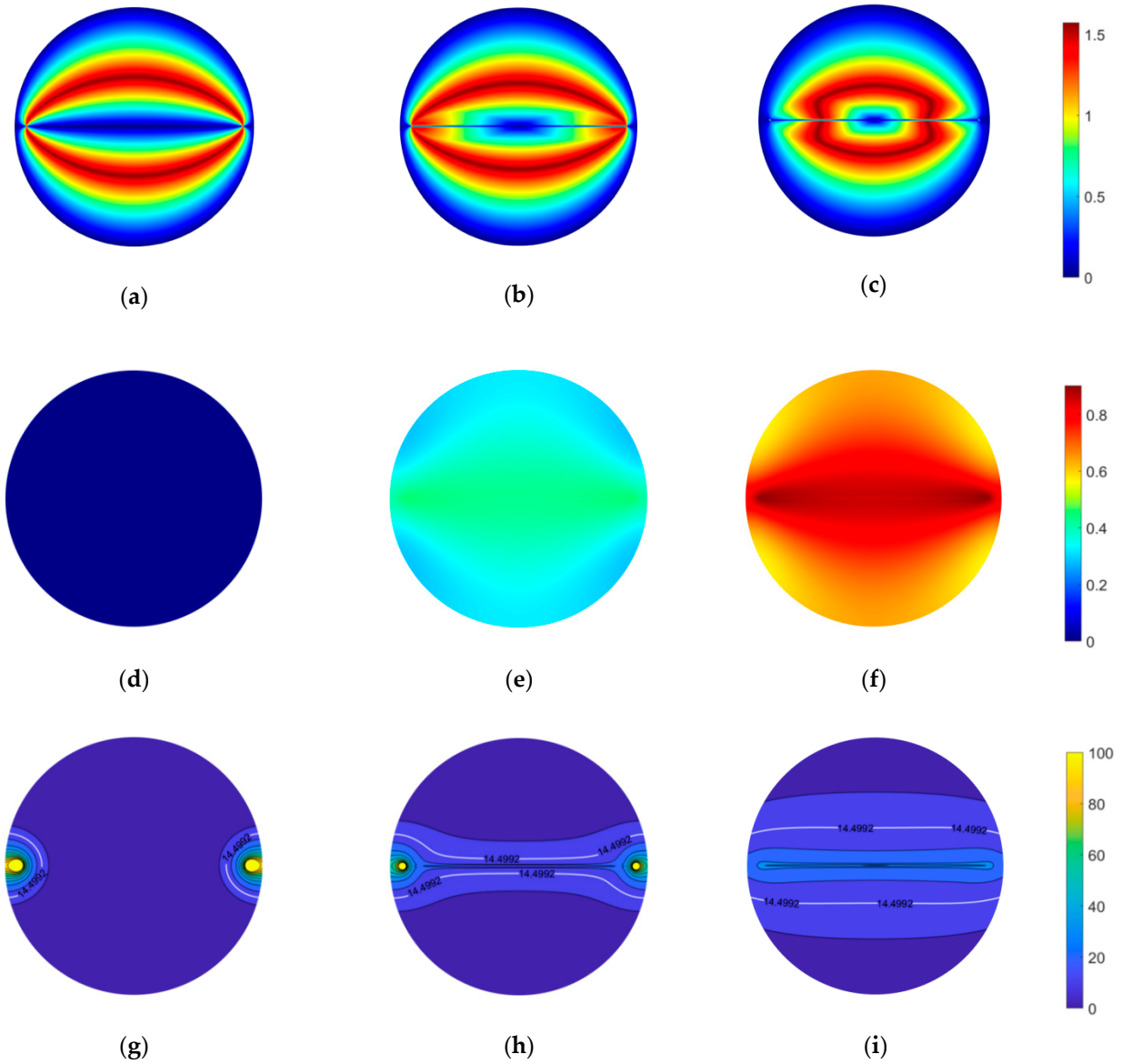

Figure 11. Time-averaged EI values over the domain for (**a**–**c**) streamline crossing and (**d**–**f**) relative rate of velocity change and (**g**–**i**) the contour of v_{sum} with μ of 1.0 and ν of 0.9. From the left, each column represents $r_{trans} = 0.0$, 0.5, and 1.0. The white line in the last row denotes v_{thresh}, equal to 14.4992. Note, the colour bar range for mobility is fixed at 0 to 100 in order to highlight the region where v_{sum} is greater than v_{thresh}.

As seen in Figures 9 and 10, the value of the relative rate of velocity change linearly increases regardless of the system parameters. Given that the velocity field has a singularity at the vortex centre, the velocity magnitude near to the centre is extremely large, and therefore the higher values of r_{trans} would result in the larger calculated values of this EI (see Figure 11d–f). As for the mobility, from Figure 11d–f and Equations (20)–(22), $\widetilde{w}$ is high around/between the vortex centres, so ν_{fast} dominates the calculation of ν_{sum} and velocity cancellation is important. For the pure blinking model, the directions of the velocity vectors by the fixed vortices are (nearly) opposite, and the differences in velocity magnitude are trivial unless the velocities are very close to the vortex centres. However, in the region around the centres where the velocities are aligned, it is not meaningful to distinguish ν_{fast} and ν_{slow} , and only the magnitude contributes to the EI. As the former effect of the continuous transition is positive and the latter would be negative, the resultant effect would be beneficial for large vortex spacing but not for the small spacing. Although a value of ν_{sum} at each point can be reduced with the continuous transition, η is computed based on

the size of the region where ν_{sum} is faster than ν_{thresh} (indicated by the white contour in Figure 11g–i). Therefore, η decreases and increases for the small and large vortex spacing, respectively. Unlike for streamline crossing, the combined effect of $\overline{\alpha}$ for large ν was not observed, as the mobility is only contingent on the region having ν_{sum} bigger than ν_{thresh}. Consequently, it could be concluded that the trend of mixing performance with small and large ν would be more likely to be predicted by the first and second c-EI, respectiely, while the mobility is expected to predict both cases.

Although such graph trends are inferred by rough explanations, and the graph shape can be somewhat different, especially for I, the expectation is, notwithstanding, quite precise in Table 1. It is observed that the mixing prediction is strong at small ν for the streamline crossing while the relative rate of velocity change shows good prediction at large ν. As for the mobility, the prediction is quite well achieved overall, but is Poor in a few cases. This could be because the inversion of the trend from small to large ν is inaccurately predicted, such as is shown in the third plots in Figures 9b and 10c. Another explanation might be that the prediction of mobility appears monotonically, so that the detailed properties of the mixing behaviour are not captured well, as seen in Figure 10d.

The product of the steamline crossing and mobility was expected to provide a better prediction than the previous two c-EIs, based on the conclusions of McIlhany and Wiggins [20], which was however found to not always be the case in this study. In Table 1, the evaluations for the product of these two quantities in bold type indicates a difference from the mobility, and the up/down arrows denote an improved/worsened prediction by the product, respectively. The improvements in prediction seem to be randomly distributed, with no clear pattern, and in some case reducing the correlation between the c-EI and mixing. Overall, mobility appears to be a better predictor of mixing performance with more Good correlations and fewer Poor.

3.3. Computational Efficiency

The high computational cost of Lagrangian mixing analysis has motivated the creation of EIs. Though they are less accurate and do not provide absolute quantification of the mixing performance, their substantially lower computational cost is attractive. For particle tracking, the run-time is dependent on the number of iterations, system period, and for this study, it was also affected by the ratio of the continuous transition, as particle tracking for the fixed vortex position was computed using Aref's mapping, which has a fixed computational cost.

The total run-time for the Lagrangian approaches ranged between 5668 s and 110,234 s while it was between 1.14 s and 686 s for the c-EIs. Although the c-EIs require a longer run-time than the d-EIs (which had an averaged run time of just 0.2034 s), c-EIs can give a more precise prediction of mixing, for both discontinuous and continuous states, than the d-EIs, for a total run time still much shorter than Lagrangian-based methods.

4. Discussion

4.1. Findings and Implications

Previous research [1,19] into the blinking vortex model highlighted that vortices placed closed together and run for a long period, led to good mixing performance, which was confirmed here for cases without continuous transition. Introducing a continuous transition phase did not improve mixing for small vortex spacing, however when mixing was poor, such as for large vortex spacing, the transition regime enhanced the interaction of these vortices and improved the mixing. Similarly, in some cases the continuous transition also improved mixing performance in systems with a shorter time period.

Such findings imply that, as in [10], a complete discontinuity is not strictly necessary for good mixing in systems based on a streamline crossing principles. This is useful for engineering applications, particularly for continuous flow pipe-based systems, where a strict discontinuity may be impossible to achieve.

Discontinuous EIs were no longer accurate once more than a small amount of continuous transition was introduced to the system. The continuous EIs, mobility and the product of the streamline crossing and mobility, in general showed good agreement with the actual mixing performance. Although it was not explicitly stated whether the latter showed a better performance than the former did in [20], it did not for this study. The prediction of mixing by this product was improved in some cases and worsened in others. In contrast to the monotonic prediction of the c-EIs, the variations of I were not as simple, due to a range of physical effects, as discussed in Section 3.1.1, which the c-EIs appear unable to capture.

4.2. Limitations and Future Work

The blinking vortex model is somewhat unrealistic in that it is inviscid and contains singularities at the vortex centres. The point vortices could be renormalised to remove these singularities, though it is expected that the overall phenomena would be preserved. A more significant limitation is that there is only a single region of closed streamlines. A more complicated flow, such as one containing at least one separatrix should be tested to see if the key findings still apply.

The system parameters and the transition motion were kept simple here. However, there are many system parameters that could be varied, for example, asymmetric vortex positioning, more than two vortices, order of vortex activation, and nonlinear trajectories of the point vortices. Appropriate manipulation of the latter variable might help to reduce the size of islands of regular flow, particularly for large vortex spacing.

The c-EIs showed good performance for predicting overall mixing behaviour in the presence of the moving vortex. However, given that the assessment conducted in Table 1 was quite generous and the c-EIs were less likely to capture finer details of the mixing, it seems that further improvements are required to Eulerian indicators so that they can capture all of the flow features that contribute to mixing.

5. Conclusions

The results showed that up to 30% transition time between discrete states was either neutral or beneficial for the mixing performance, with the biggest benefit observed for cases where the mixing from the blinking protocol was poor, e.g., due to large vortex spacing. The biggest improvement in mixing, observed for r_{trans} of 0.2, was an increase of 62.4% when $\mu = 1.0$ and $\nu = 0.9$, while the worsened performance for $\nu = 0.1$ was less than 5%. This effect was generally consistent across the different blinking periods although very short blinking periods did not follow the same trend. Finally, for this system, mobility was the EI that most accurately characterised the mixing performance. However, there were still some parameter cases where its agreement with actual mixing performance was poor, with the EIs unable to capture the benefits of this small amount of transition, suggesting that improved EIs may be needed. Overall, these results suggest that mixing systems, such as continuous pipe flow-based devices, which are designed assuming a discontinuous change in velocity, might actually benefit from the presence of a small degree of continuous transition between discrete states.

Supplementary Materials: The following are available online at https://www.mdpi.com/2311-5521/6/1/10/s1, MATLAB code for performing particle tracking, generating Poincaré sections, and computing Eulerian indicators.

Author Contributions: Conceptualisation, H.R. and A.N.C.; methodology, H.R. and A.N.C.; software, H.R.; validation, H.R.; formal analysis, H.R. and A.N.C.; investigation, H.R.; writing—original draft preparation, H.R. and A.N.C.; writing—review and editing, H.R. and A.N.C.; visualisation, H.R.; supervision, A.N.C. All authors have read and agreed to the published version of the manuscript.

Funding: This research received no external funding.

Institutional Review Board Statement: Not applicable.

Informed Consent Statement: Not applicable.

Data Availability Statement: Code used to generate the data in this paper is available for download in the supplementary materials. Specific instances of this data are available on request from the corresponding author.

Conflicts of Interest: The authors declare no conflict of interest.

References

1. Aref, H. Stirring by chaotic advection. *J. Fluid Mech.* **1984**, *143*, 1–21. [CrossRef]
2. Khakhar, D.V.; Franjione, J.G.; Ottino, J.M. A case study of chaotic mixing in deterministic flows: The partitioned-pipe mixer. *Chem. Eng. Sci.* **1987**, *42*, 2909–2926. [CrossRef]
3. Ling, F.H. Chaotic mixing in a spatially periodic continuous mixer. *Phys. Fluids Fluid Dyn.* **1993**, *5*, 2147–2160. [CrossRef]
4. Mizuno, Y.; Funakoshi, M. Chaotic mixing caused by an axially periodic steady flow in a partitioned-pipe mixer. *Fluid Dyn. Res.* **2004**, *35*, 205. [CrossRef]
5. Jung, H.I.; Jung, S.Y.; Kang, T.G.; Ahn, K.H. Numerical study on the mixing in a barrier-embedded partitioned pipe mixer (BPPM) for non-creeping flow conditions. *Korea-Aust. Rheol. J.* **2018**, *30*, 227–238. [CrossRef]
6. Jones, S.W.; Thomas, O.M.; Aref, H. Chaotic advection by laminar flow in a twisted pipe. *J. Fluid Mech.* **1989**, *209*, 335–357. [CrossRef]
7. Jen, C.-P.; Wu, C.-Y.; Lin, Y.-C.; Wu, C.-Y. Design and simulation of the micromixer with chaotic advection in twisted microchannels. *Lab. Chip* **2003**, *3*, 77–81. [CrossRef]
8. Schönfeld, F.; Hardt, S. Simulation of helical flows in microchannels. *AIChE J.* **2004**, *50*, 771–778. [CrossRef]
9. Jiang, F.; Drese, K.S.; Hardt, S.; Küpper, M.; Schönfeld, F. Helical flows and chaotic mixing in curved micro channels. *AIChE J.* **2004**, *50*, 2297–2305. [CrossRef]
10. Cookson, A.N.; Doorly, D.J.; Sherwin, S.J. Efficiently Generating Mixing by Combining Differing Small Amplitude Helical Geometries. *Fluids* **2019**, *4*, 59. [CrossRef]
11. Ottino, J.M. *The Kinematics of Mixing: Stretching, Chaos, and Transport*; Cambridge University Press: Cambridge, UK, 1989; ISBN 0-521-36335-7.
12. Cookson, A.N.; Doorly, D.J.; Sherwin, S.J. Mixing Through Stirring of Steady Flow in Small Amplitude Helical Tubes. *Ann. Biomed. Eng.* **2009**, *37*, 710–721. [CrossRef] [PubMed]
13. Chien, W.-L.; Rising, H.; Ottino, J.M. Laminar mixing and chaotic mixing in several cavity flows. *J. Fluid Mech.* **1986**, *170*, 355–377. [CrossRef]
14. Stroock, A.D.; Dertinger, S.K.W.; Ajdari, A.; Mezic, I.; Stone, H.A.; Whitesides, G.M. Chaotic Mixer for Microchannels. *Science* **2002**, *295*, 647–651. [CrossRef] [PubMed]
15. Kim, D.S.; Lee, S.W.; Kwon, T.H.; Lee, S.S. A barrier embedded chaotic micromixer. *J. Micromech. Microeng.* **2004**, *14*, 798. [CrossRef]
16. McIlhany, K.L.; Wiggins, S. Optimizing mixing in channel flows: Kinematic aspects associated with secondary flows in the cross-section. *Microfluid. Nanofluidics* **2011**, *10*, 249–262. [CrossRef]
17. Hossain, S.; Lee, I.; Kim, S.M.; Kim, K.-Y. A micromixer with two-layer serpentine crossing channels having excellent mixing performance at low Reynolds numbers. *Chem. Eng. J.* **2017**, *327*, 268–277. [CrossRef]
18. Sturman, R.; Ottino, J.M.; Wiggins, S. *The Mathematical Foundations of Mixing: The Linked Twist Map as a Paradigm in Applications: Micro to Macro, Fluids to Solids*; Cambridge University Press: Cambridge, UK, 2006; ISBN 978-0-521-86813-6.
19. Sturman, R.; Wiggins, S. Eulerian indicators for predicting and optimizing mixing quality. *New J. Phys.* **2009**, *11*, 075031. [CrossRef]
20. McIlhany, K.L.; Wiggins, S. Eulerian indicators under continuously varying conditions. *Phys. Fluids* **2012**, *24*, 073601. [CrossRef]
21. McIlhany, K.L.; Guth, S.; Wiggins, S. Lagrangian and Eulerian analysis of transport and mixing in the three dimensional, time dependent Hill's spherical vortex. *Phys. Fluids* **2015**, *27*, 063603. [CrossRef]
22. McIlhany, K.L.; Mott, D.; Oran, E.; Wiggins, S. Optimizing mixing in lid-driven flow designs through predictions from Eulerian indicators. *Phys. Fluids* **2011**, *23*, 082005. [CrossRef]
23. Reza, M.M.S.; Arzani, A. A critical comparison of different residence time measures in aneurysms. *J. Biomech.* **2019**, *88*, 122–129. [CrossRef] [PubMed]